BLACK-BOX ADVERSARIAL ATTACK WITH TRANSFERABLE MODEL-BASED EMBEDDING

Anonymous authors
Paper under double-blind review

ABSTRACT

We present a new method for black-box adversarial attack. Unlike previous methods that combined transfer-based and scored-based methods by using the gradient or initialization of a surrogate white-box model, this new method tries to learn a low-dimensional embedding using a pretrained model, and then performs efficient search within the embedding space to attack an unknown target network. The method produces adversarial perturbations with high level semantic patterns that are easily transferable. We show that this approach can greatly improve the query efficiency of black-box adversarial attack across different target network architectures. We evaluate our approach on MNIST, ImageNet and Google Cloud Vision API, resulting in a significant reduction on the number of queries. We also attack adversarially defended networks on CIFAR10 and ImageNet, where our method not only reduces the number of queries, but also improves the attack success rate.

1 INTRODUCTION

The wide adoption of neural network models in modern applications has caused major security concerns, as such models are known to be vulnerable to adversarial examples that can fool neural networks to make wrong predictions (Szegedy et al., 2014). Methods to attack neural networks can be divided into two categories based on whether the parameters of the neural network are assumed to be known to the attacker: white-box attack and black-box attack. There are several approaches to find adversarial examples for black-box neural networks. The transfer-based attack methods first pretrain a source model and then generate adversarial examples using a standard white-box attack method on the source model to attack an unknown target network (Goodfellow et al., 2015; Madry et al., 2018; Carlini & Wagner, 2017; Papernot et al., 2016a). The score-based attack requires a loss-oracle, which enables the attacker to query the target network at multiple points to approximate its gradient. The attacker can then apply the white-box attack techniques with the approximated gradient (Chen et al., 2017; Ilyas et al., 2018; Tu et al., 2018).

A major problem of the transfer-based attack is that it can not achieve very high success rate. And transfer-based attack is weak in targeted attack. On the contrary, the success rate of score-based attack has only small gap to the white-box attack but it requires many queries. Thus, it is natural to combine the two black-box attack approaches, so that we can take advantage of a pretrained white-box source neural network to perform more efficient search to attack an unknown target black-box model.

In fact, in the recent NeurIPS 2018 Adversarial Vision Challenge (Brendel et al., 2018), many teams transferred adversarial examples from a source network as the starting point to carry out black-box boundary attack (Brendel et al., 2017). $\mathcal{N}$Attack also used a regression network as initialization in the score-based attack (Li et al., 2019). The transferred adversarial example could be a good starting point that lies close to the decision boundary for the target network and accelerate further optimization. P-RGF (Cheng et al., 2019) used the gradient information from the source model to accelerate searching process. However, gradient information is localized and sometimes it is misleading. In this paper, we push the idea of using a pretrained white-box source network to guide black-box attack significantly further, by proposing a method called TRansferable EMbedding based Black-box Attack (TREMBA). TREMBA contains two stages: (1) train an encoder-decoder that can effectively generate adversarial perturbations for the source network with a low-dimensional embedding space; (2) apply NES to the low-dimensional embedding space of the pretrained generator to search adversarial examples for the target network. TREMBA uses global information of the source model, capturing high level semantic adversarial features that are insensitive to different models. Unlike noise-like perturbations, such perturbations would have much higher transferablity across different models. Therefore we could gain query efficiency by performing queries in the embedding space.

We note that there have been a number of earlier works on using generators to produce adversarial perturbations in the white-box setting (Baluja & Fischer, 2018; Xiao et al., 2018; Wang & Yu, 2019). While black-box attacks were also considered there, they focused on training generators with dynamic distillation. These early approaches required many queries to fine-tune the classifier for different target networks, which may not be practical for real applications. While our approach also relies on a generator, we train it as an encoder-decoder that produces a low-dimensional embedding space. By applying a standard black-box attack method such as NES on the embedding space, adversarial perturbations can be found efficiently for a target model.

It is worth noting that the embedding approach has also been used in AutoZOOM (Tu et al., 2018). However, it only trained the autoencoder to reconstruct the input, and it did not take advantage of the information of a pretrained network. Although it also produces structural perturbations, these perturbations are usually not suitable for attacking regular networks and sometimes its performance is even worse than directly applying NES to the images (Cheng et al., 2019; Guo et al., 2019). TREMBA, on the other hand, tries to learn an embedding space that can efficiently generate adversarial perturbations for a pretrained source network. Compared to AutoZOOM, our new method produces adversarial perturbation with high level semantic features that could hugely affect arbitrary target networks, resulting in significantly lower number of queries.

We summarize our contributions as follows:

1. We propose TREMBA, an attack method that explores a novel way to utilize the information of a pretrained source network to improve the query efficiency of black-box attack on a target network.
2. We show that TREMBA can produce adversarial perturbations with high level semantic patterns, which are effective across different networks, resulting in much lower queries on MNIST and ImageNet especially for the targeted attack that has low transferablity.
3. We demonstrate that TREMBA can be applied to SOTA defended models (Madry et al., 2018; Xie et al., 2018). Compared with other black-box attacks, TREMBA increases success rate by approximately 10% while reduces the number of queries by more than 50%.

2 Related Works

There have been a vast literature on adversarial examples. We will cover the most relevant topics including white-box attack, black-box attack and defense methods.

White-Box Attack White-box attack requires the full knowledge of the target model. It was first discovered by (Szegedy et al., 2014) that adversarial examples could be found by solving an optimization problem with L-BFGS (Nocedal, 1980). Later on, other methods were proposed to find adversarial examples with improved success rate and efficiency (Goodfellow et al., 2015; Kurakin et al., 2016; Papernot et al., 2016b; Moosavi-Dezfooli et al., 2016). More recently, it was shown that generators can also construct adversarial noises with high success rate (Xiao et al., 2018; Baluja & Fischer, 2018).

Black-Box Attack Black-box attack can be divided into three categories: transfer-based, score-based and decision-based. It is well known that adversaries have high transferablity across different networks (Papernot et al., 2016a). Transfer-based methods generate adversarial noises on a source model and then transfer it to an unknown target network. Targeted attack is much harder for un-targeted attack for transfer-based method. (Liu et al., 2016) used an ensemble as source model, largely improving the success rate for transfer-based targeted attack. Score-based attack assumes that the attacker can query the output scores of the target network. The attacker usually uses sampling methods to approximate the true gradient (Chen et al., 2017; Ilyas et al., 2018; Li et al., 2019). AutoZOOM tried to improve the query efficiency by reducing the sampling space with a bilinear transformation or an autoencoder (Tu et al., 2018). In decision-based attack, the attacker only knows the output label of the classifier. Boundary attack and its variants are very powerful in this setting (Brendel et al., 2017; Dong et al., 2019). In NeutIPS 2018 Adversarial Vision Challenge (Brendel et al., 2018), some teams combined transfer-based attack and decision-based attack in their attacking methods (Brunner et al., 2018). And in a similar spirit, $\mathcal{N}$Attack also used a regression network as initialization in score-based attack (Li et al., 2019). Gradient information from the surrogate model could also be used to accelerate the scored-based attack (Cheng et al., 2019) .

Defense Methods Several methods have been proposed to overcome the vulnerability of neural networks. Gradient masking based methods add non-differential operations in the model, interrupting the backward pass of gradients. However, they are vulnerable to adversarial attacks with the approximated gradient (Athalye et al., 2018; Li et al., 2019). Adversarial training is the SOTA method that can be used to improve the robustness of neural networks. Adversarial training is a minimax game. The outside minimizer performs regular training of the neural network, and the inner maximizer finds a perturbation of the input to attack the network. The inner maximization process can be approximated with FGSM (Goodfellow et al., 2015), PGD (Madry et al., 2018), adversarial generator (Wang & Yu, 2019) etc. Moreover, feature denoising can improve the robustness of neural networks on ImageNet (Xie et al., 2018).

3 Black-Box Adversarial Attack with Generator

Consider a DNN classifier $F(x)$. Let $x \in [0,1]^{\dim(x)}$ be an input, and let $F(x)$ be the output vector obtained before the softmax layer. We denote $F(x)_i$ as the i-th component for the output vector and y as the label for the input. For un-targeted attack, our goal is to find a small perturbation δ such that the classifier predicts the wrong label, i.e. $\arg\max\ F(x+\delta) \neq y$. And for targeted attack, we want the classifier to predicts the target label t, i.e. $\arg\max\ F(x+\delta) = t$. The perturbation δ is usually bounded by ℓ_p norm: $\|\delta\|_p \leq \varepsilon$, with a small $\varepsilon > 0$.

Adversarial perturbations often have high transferablity across different DNNs. Given a white-box source DNN F_s with known architecture and parameters, we can transfer its white-box adversarial perturbation δ_s to a black-box target DNN F_t with reasonably good success rate. It is known that even if $x + \delta_s$ fails to be an adversarial example, δ_s can still act as a good starting point for searching adversarial examples using a score-based attack method. This paper shows that the information of F_s can be further utilized to train a generator, and performing search on its embedding space leads to more efficient black-box attacks of an unknown target network F_t.

3.1 Generating Adversarial Perturbations with Generator

Adversarial perturbations can be generated by a generator network $\mathcal{G}$. We explicitly divide the generator into two parts: an encoder $\mathcal{E}$ and a decoder $\mathcal{D}$. The encoder takes the origin input x and output a latent vector $z = \mathcal{E}(x)$, where $\dim(z) \ll \dim(x)$. The decoder takes z as the input and outputs an adversarial perturbation $\delta = \varepsilon \tanh(\mathcal{D}(z))$ with $\dim(\delta) = \dim(x)$. In our new method, we will train the generator $\mathcal{G}$ so that $\delta = \varepsilon \tanh(\mathcal{G}(x))$ can fool the source network F_s.

Suppose we have a training set $\{(x_1, y_1), \ldots, (x_n, y_n)\}$, where x_i denotes the input and y_i denotes its label. For un-targeted attack, we train the desired generator by minimizing the following hinge loss (Carlini & Wagner, 2017):

$$\mathcal{L}_{\text{untarget}}(x_i, y_i) = \max\left(F_s(\varepsilon \tanh(\mathcal{G}(x_i)) + x_i)_{y_i} - \max_{j \neq y_i} F_s(\varepsilon \tanh(\mathcal{G}(x_i)) + x_i)_j, -\kappa\right), \quad (1)$$

And for targeted, we use

$$\mathcal{L}_{\text{target}}(x_i, t) = \max\left(\max_{j \neq y_i} F_s(\varepsilon \tanh(\mathcal{G}(x_i)) + x_i)_j - F_s(\varepsilon \tanh(\mathcal{G}(x_i)) + x_i)_t, -\kappa\right), \quad (2)$$

where t denotes the targeted class and κ is the margin parameter that can be used to adjust transferability of the generator. A higher value of κ leads to higher transferability to other models. We focus on ℓ_∞ norm in this work. By adding point-wise $\tanh$ function to an unnormalized output $\mathcal{D}(z)$, and scaling it with ε, $\delta = \varepsilon \tanh(\mathcal{D}(z))$ is already bounded as $\|\delta\|_\infty < \varepsilon$. Therefore we employ this transformation, so that we do not need to impose the infinity norm constraint explicitly.

3.2 Search over latent space with NES

Given a new black-box DNN classifier $F_t(x)$, for which we can only query its output at any given point x. As in (Ilyas et al., 2018), we can employ NES to approximate the gradient of a properly defined surrogate loss in order to find an adversarial example. Denote the surrogate loss by $\mathcal{L}$, then we may use the following equation to iteratively update δ:

$$\delta_{t+1} = \prod_{[-\varepsilon,\varepsilon]} (\delta_t - \eta \cdot \text{sign}(\frac{1}{b}\sum_{k=1}^{b} \mathcal{L}(x+\omega_k, y)\nabla \log \mathcal{N}(\omega_k|\delta_t, \sigma^2))), \tag{3}$$

where η is the learning rate, b is the minibatch sample size, and $\prod_{[-\varepsilon,\varepsilon]}$ represents a clipping operation, which projects δ onto the ℓ_∞ ball. The sign function provides an approximation of the gradient, which reduces the estimation variance. However, it is observed that more effective attacks can be obtained by removing the sign function (Li et al., 2019). Therefore in this work, we remove the sign function from Eqn (3) and directly use the estimated gradient.

Instead of performing search on the input space, TREMBA performs search on the embedding space z. The generator $\mathcal{G}$ explores the weakness of the source DNN F_s so that $\mathcal{D}$ produces perturbations that can effective attack F_s. For a different unknown target network F_t, we show that our method can still generate perturbations leading to more effective attack of F_t. Given an input x and its label y, we choose a starting point $z^0 = \mathcal{E}(x)$. The gradient of z^t given by NES can be estimated as:

$$\begin{aligned}\nabla_{z^t}\mathcal{L}(x+\varepsilon\tanh(\mathcal{D}(z^t)), y) &\approx \nabla_{z^t}\mathbb{E}_{\nu\sim\mathcal{N}(z^t,\sigma^2)}\left[\mathcal{L}(x+\varepsilon\tanh(\mathcal{D}(\nu)), y)\right] \qquad (4)\\ &\approx \frac{1}{b}\sum_{k=1}^{b}\mathcal{L}(x+\varepsilon\tanh(\mathcal{D}(\nu_k)), y)\nabla_{z^t}\log\mathcal{N}(\nu_k|z^t,\sigma^2).\end{aligned}$$

Moreover, z^t is updated with stochastic gradient descent. The detailed procedure is presented in Algorithm 1. We do not need to do projection explicitly since δ already satisfies $\|\delta\|_\infty < \varepsilon$.

Next we shall briefly explain why applying NES on the embedding space z can accelerate the search process. Adversarial examples can be viewed as a distribution lying around a given input. Usually this distribution is concentrated on some small regions, making the search process relatively slow. After training on the source network, the adversarial perturbations of TREMBA would have high level semantic patterns that are likely to be adversarial patterns of the target network. Therefore searching over z is like searching adversarial examples in a lower dimensional space containing likely adversarial patterns. The distribution of adversarial perturbations in this space is much less concentrated. It is thus much easier to find effective adversarial patterns in the embedding space.

Algorithm 1 Black-Box adversarial attack on the embedding space

```
Input:
    Target Network $F_t$; Input $x$ and its label $y$ or the target class $t$; Encoder $\mathcal{E}$; Decoder $\mathcal{D}$; Standard deviation $\sigma$; Learning rate $\eta$; Sample size $b$; Iterations $T$; Bound for adversarial perturbation $\varepsilon$
Output: Adversarial perturbation $\delta$
$z_0 = \mathcal{E}(x)$
for $t = 1$ to $T$ do
    Sample Gaussian noise $\nu_1, \nu_2, \cdots, \nu_b \sim \mathcal{N}(z_{t-1}, \sigma^2)$
    Calculate $\mathcal{L}_i = \mathcal{L}_{\text{untarget}}(x, y)$ or $\mathcal{L}_{\text{target}}(x, t)$
    Update $z_t = z_{t-1} - \frac{\eta}{b}\sum_{i=1}^{b}\mathcal{L}_i$
end for
return $\delta = \varepsilon\tanh(\mathcal{D}(z_T))$
```

4 Experiments

We evaluated the number of queries versus success rate of TREMBA on undefended network in two datasets: MNIST (LeCun et al., 1998) and ImageNet (Russakovsky et al., 2015). Moreover, we evaluated the efficiency of our method on adversarially defended networks in CIFAR10 (Krizhevsky & Hinton, 2009) and ImageNet. We also attacked Google Cloud Vision API to show TREMBA can

Table 1: Success rate and average queries of un-targeted attack on MNIST. $\varepsilon = 0.2$

Attack	ConvNet1		ConvNet2		FCNet	
	Success	Queries	Success	Queries	Success	Queries
NES	97.88%	4380	90.32%	5428	99.98%	1183
Trans-NES$_{\text{PGD}}$	**98.65%**	2113	90.22%	4691	**99.99%**	818
Trans-NES$_{\text{FGSM}}$	98.34%	3592	91.32%	4218	99.99%	1540
AutoZOOM	93.39%	5874	91.21%	2645	99.69%	823
P-RGF	68.53%	16135	39.85%	29692	90.42%	8289
Trans-P-RGF	66.34%	16428	27.57%	35576	68.39%	18818
TREMBA	98.00%	**1064**	**92.63%**	**1359**	99.75%	**470**

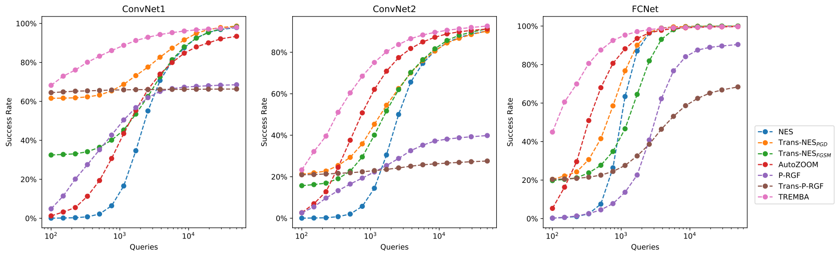

Figure 1: Success rate of un-targeted attack at different query levels for undefended MNIST models.

generalize to truly black-box model. We used the hinge loss from Eqn 1 and 2 as the surrogate loss for un-targeted and targeted attack respectively.

We compared TREMBA to four methods: (1) **NES**: Method introduced by (Ilyas et al., 2018), but without the sign function for reasons explained earlier. (2) **Trans-NES**: Take an adversarial perturbation generated by PGD or FGSM on the source model to initialize NES. (3) **AutoZOOM**: Attack target network with an unsupervised autoencoder described in (Tu et al., 2018). For fair comparisons with other methods, the strategy of choosing sample size was removed. (4) **P-RGF**: Prior-guided random gradient-free method proposed in (Cheng et al., 2019). The P-RGF$_{\text{D}}(\lambda^*)$ version was compared. We also combined P-RGF with initialization from Trans-NES$_{\text{PGD}}$ to form a more efficient method for comparison, denoted by Trans-P-RGF.

Since different methods achieve different success rates, we need to compare their efficiency at different levels of success rate. For method i with success rate s_i, the average number of queries is q_i for all success examples. Let q^* denote the upper limit of queries, we modified the average number of queries to be $q_i^* = [(\max_j s_j - s_i) \cdot q^* + s_i \cdot q_i] / \max_j s_j$, which unified the level of success rate and treated queries of failure examples as the upper limit on the number of queries. Average queries sometimes could be misleading due to the the heavy tail distribution of queries. Therefore we plot the curve of success rate at different query levels to show the detailed behavior of different attacks.

The upper limit on the number of queries was set to 50000 for all datasets, which already gave very high success rate for nearly all the methods. Only correctly classified images were counted towards success rate and average queries. And to fairly compare these methods, we chose the sample size to be the same for all methods. We also added momentum and learning decay for optimization. And we counted the queries as one if its starting point successfully attacks the target classifier. The learning rate was fine-tuned for all algorithms. We listed the hyperparameters and architectures of generators and classifiers in Appendix B and C.

4.1 Black-box Attack on MNIST

We trained four neural networks on MNIST, denoted by ConvNet1, ConvNet1*, ConvNet2 and FCNet. ConvNet1* and ConvNet1 have the same architecture but different parameters. All the network achieved about 99% accuracy. The generator $\mathcal{G}$ was trained on ConvNet1* using all images from the training set. Each attack was tested on images from the MNIST test set. The limit of ℓ_∞ was $\varepsilon = 0.2$.

Table 2: Success rate and average queries of black-box targeted attack on ImageNet. Targeted class is class 0 (tench). $\varepsilon = 0.03125$

Attack	VGG19		Resnet34		DenseNet121		MobilenetV2	
	Success	Queries	Success	Queries	Success	Queries	Success	Queries
NES	94.86%	12283	93.89%	14418	95.65%	12538	97.76%	10276
Trans-NES$_{\text{PGD}}$	96.26%	6854	95.97%	8737	96.59%	8627	98.04%	9375
Trans-NES$_{\text{FGSM}}$	90.85%	12885	91.81%	14090	93.61%	12859	97.48%	9983
AutoZOOM	25.80%	40195	26.25%	39681	31.98%	37628	27.03%	39689
P-RGF	96.12%	6951	90.28%	10221	91.84%	11563	88.94%	14596
Trans-P-RGF	98.06%	2262	93.61%	6309	94.69%	7263	91.60%	10048
TREMBA	**98.47%**	**853**	**96.38%**	**1206**	**98.50%**	**1124**	**99.16%**	**1210**

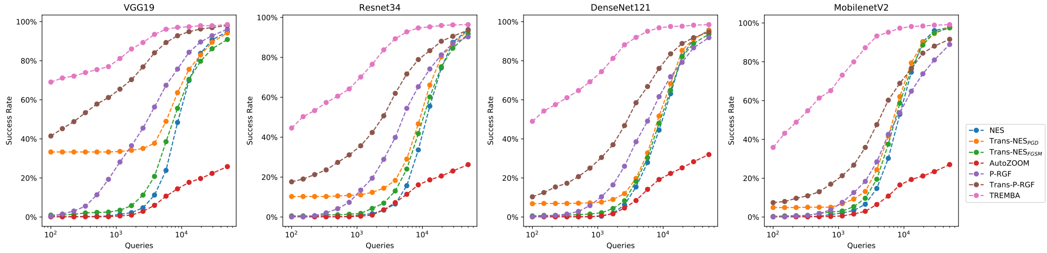

Figure 2: The success rate of black-box adversarial targeted attack at different query levels for ImageNet models. The targeted class is tench

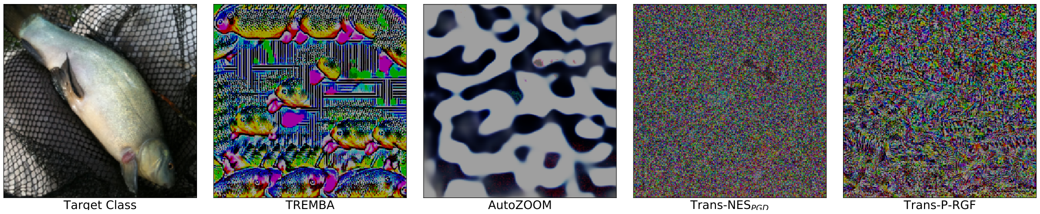

Figure 3: Visualization of adversarial perturbations targeted at tench

We performed un-targeted attack on MNIST. Table 1 lists the success rate and the average queries. Although the success rate of TREMBA is slightly lower than Trans-NES in ConvNet1 and FCNet, their success rate are already close to 100% and TREMBA achieves about 50% reduction of queries compared with other attacks. In contrast to efficient attack on ImageNet, P-RGF and Trans-P-RGF behaves very bad on MNIST. Figure 4 shows that TREMBA consistently achieves higher success rate at nearly all query levels.

4.2 Black-Box Attack on ImageNet

We randomly divided the ImageNet validation set into two parts, containing 49000 and 1000 images respectively. The first part was used as the training data for the generator $\mathcal{G}$, and the second part was used for evaluating the attacks. We evaluated the efficiency of all adversarial attacks on VGG19 (Simonyan & Zisserman, 2014), Resnet34 (He et al., 2016), DenseNet121 (Huang et al., 2017) and MobilenetV2 (Sandler et al., 2018). All networks were downloaded using *torchvision* package. We set $\varepsilon = 0.03125$.

Following (Liu et al., 2016), we used an ensemble (VGG16, Resnet18, Squeezenet (Iandola et al., 2016) and Googlenet (Szegedy et al., 2015)) as the source model to improve transferablity (Liu et al., 2016) for both targeted and un-targeted attack. TREMBA, Trans-NES, P-RGF and Trans-P-RGF all used the same source model for fair comparison. We chose several target class. Here, we show the result of attacking class 0 (tench) in Table 2 and Figure 2. And we leave the result of attacking other classes in Appendix A.1. The average queries for TREMBA is about 1000 while nearly all the average queries for other methods are more than 6000. TREMBA also achieves much lower queries for un-targeted attack on ImageNet. The result is shown in Appendix A.2 due to space limitation.

Figure 3 shows the adversarial perturbations of different methods. Unlike adversarial perturbations produced by PGD, the perturbations of TREMBA reflect some high level semantic patterns of the targeted class such as the fish scale. As neural networks usually capture such patterns for classification, the adversarial perturbation of TREMBA would be more easy to transfer than the noise-like perturbation produced by PGD. Therefore TREMBA can search very effectively for the target network. More examples of perturbations of TREMBA are shown in Appendix A.3.

Choice of ensemble: We performed attack on different ensembles of source model, which is shown in Appendix A.4. TREMBA outperforms the other methods in different ensemble model. And more source networks lead to better transferability for TREMBA, Trans-NES and Trans-P-RGF.

Varying ε: We also changed ε and performed attack on $\varepsilon = 0.02$ and $\varepsilon = 0.04$. As shown in Appendix A.5, TREMBA still outperforms the other methods despite using the $\mathcal{G}$ trained on $\varepsilon = 0.03125$.

Sample size and dimension the embedding space: To justify the choice of sample size, we performed a hyperparameter sweep over b and the result is shown in Appendix A.6. And we also changed the dimension of the embedding space for AutoZOOM and Trans-P-RGF. As shown in Appendix A.7, the performance gain of TREMBA does not purely come from the diminishing of dimension of the embedding space.

4.3 Black-Box Attack on Defended Models

This section presents the results for attacking defended networks. We performed un-targeted attack on two SOTA defense methods on CIFAR10 and ImageNet. MNIST is not studied since it is already robust against very strong white-box attacks. For CIFAR10, the defense model was going through PGD minimax training (Madry et al., 2018). We directly used their model as the source network[1], denoted by WResnet. To test whether these methods can transfer to a defended network with a different architecture, we trained a defended ResNeXt (Xie et al., 2017) using the same method. For ImageNet, we used the SOTA model[2] from (Xie et al., 2018). We used "ResNet152 Denoise" as the source model and transfered adversarial perturbations to the most robust "ResNeXt101 DenoiseAll". Following the previous settings, we set $\varepsilon = 0.03125$ for both CIFAR10 and ImageNet.

As shown in Table 3, TREMBA achieves higher success rates with lower number of queries. TREMBA achieves about 10% improvement of success rate while the average queries are reduced by more than 50% on ImageNet and by 80% on CIFAR10. The curves in Figure 4(a) and 4(b) show detailed behaviors. The performance of AutoZOOM surpasses Trans-NES on defended models. We suspect that low-frequency adversarial perturbations produced by AutoZOOM will be more suitable to fool the defended models than the regular networks. However, the patterns learned by AutoZOOM are still worse than adversarial patterns learned by TREMBA from the source network.

An optimized starting point for TREMBA: $z_0 = \mathcal{E}(x)$ is already a good starting point for attacking undefended networks. However, the capability of generator is limited for defended networks (Wang & Yu, 2019). Therefore, z_0 may not be the best starting point we can get from the defended source network. To enhance the usefulness of the starting point, we optimized z on the source network by gradient descent and found

$$z_0^* = \arg\min_z \max\left(F_s(\varepsilon \tanh(\mathcal{D}(z)) + x)_y - \max_{j\neq y_i} F_s(\varepsilon \tanh(\mathcal{D}(z)) + x)_j, -\kappa\right). \tag{5}$$

The method is denoted by TREMBA$_{\text{OSP}}$ (TREMBA with optimized starting point). Figure 4 shows TREMBA$_{\text{OSP}}$ has higher success rate at small query levels, which means its starting point is better than TREMBA.

[1] https://github.com/MadryLab/cifar10_challenge

[2] https://github.com/facebookresearch/ImageNet-Adversarial-Training

Table 3: Success rate of average queries of black-box un-targeted attack on defended CIFAR10 and ImageNet model. Source network is WResNet and ResNet152 Denoise.

Attack	CIFAR10 ResneXt		ImageNet RexneXt101 DenoiseAll	
	Success	Queries	Success	Queries
NES	32.17%	24521	29.72%	26526
Trans-NES$_{\text{PGD}}$	32.92%	20735	32.84%	20446
Trans-NES$_{\text{FGSM}}$	33.17%	20873	33.66%	18547
AutoZOOM	33.70%	14870	38.75%	14605
P-RGF	22.37%	25818	32.51%	17926
Trans-P-RGF	20.88%	27222	31.03%	19262
TREMBA	**42.73%**	**2528**	49.59%	5985
TREMBA$_{\text{OSP}}$	41.56%	4994	**50.41%**	**4771**

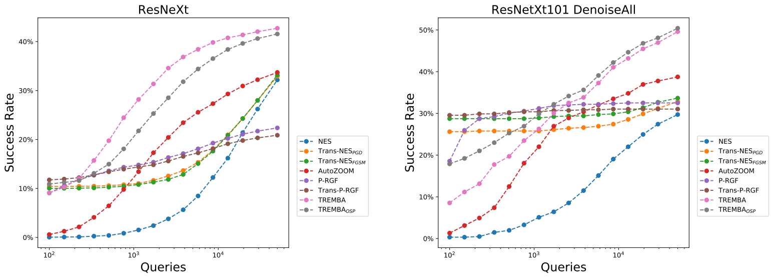

(a) CIFAR10

(b) ImageNet

Figure 4: The success rate at different query levels for defended CIFAR10 and ImageNet models. (a)CIFAR10; (b)ImageNet.

Table 4: Success rate and average queries of un-targeted attack of 10 images on Google Vision API.

Method	NES	AutoZOOM	Trans-NES$_{\text{PGD}}$	P-RGF	Trans-P-RGF	TREMBA
Success	70.00%	20.00%	70.00%	50.00%	60.00%	90.00%
Queries	245	410	114	324	167	8

4.4 Attack Google Cloud Vision API

We also attacked the Google Cloud Vision API, which was much harder to attack than the single neural network. Therefore we set $\varepsilon = 0.05$ and perform un-targeted attack on the API, changing the top1 label to whatever is not on top1 before. We chose 10 images for the ImageNet dataset and set query limit to be 500 due to high cost to use the API. As shown Table 4, TREMBA achieves much higher accuracy success rate and lower number of queries. We show the example of successfully attacked image in Appendix A.8.

5 Conclusion

We propose a novel method, TREMBA, to generate likely adversarial patterns for an unknown network. The method contains two stages: (1) training an encoder-decoder to generate adversarial perturbations for the source network; (2) search adversarial perturbations on the low-dimensional embedding space of the generator for any unknown target network. Compared with SOTA methods, TREMBA learns an embedding space that is more transferable across different network architectures. It achieves two to six times improvements in black-box adversarial attacks on MNIST and ImageNet and it is especially efficient in performing targeted attack. Furthermore, TREMBA demonstrates great capability in attacking defended networks, resulting in a nearly 10% improvement on the attack success rate, with two to six times of reductions in the number of queries. TREMBA opens up new ways to combine transfer-based and score-based attack methods to achieve higher efficiency in searching adversarial examples.

References

Anish Athalye, Nicholas Carlini, and David A. Wagner. Obfuscated gradients give a false sense of security: Circumventing defenses to adversarial examples. In *Proceedings of the 35th International Conference on Machine Learning, ICML 2018*, 2018. URL `http://proceedings.mlr.press/v80/athalye18a.html`.

Shumeet Baluja and Ian Fischer. Learning to attack: Adversarial transformation networks. In *Proceedings of AAAI-2018*, 2018. URL `http://www.esprockets.com/papers/aaai2018.pdf`.

Wieland Brendel, Jonas Rauber, and Matthias Bethge. Decision-based adversarial attacks: Reliable attacks against black-box machine learning models. *arXiv preprint arXiv:1712.04248*, 2017.

Wieland Brendel, Jonas Rauber, Alexey Kurakin, Nicolas Papernot, Behar Veliqi, Marcel Salathé, Sharada P Mohanty, and Matthias Bethge. Adversarial vision challenge. In *32nd Conference on Neural Information Processing Systems (NIPS 2018) Competition Track*, 2018. URL `https://arxiv.org/abs/1808.01976`.

Thomas Brunner, Frederik Diehl, Michael Truong Le, and Alois Knoll. Guessing smart: Biased sampling for efficient black-box adversarial attacks. *arXiv preprint arXiv:1812.09803*, 2018.

Nicholas Carlini and David Wagner. Towards evaluating the robustness of neural networks. In *2017 IEEE Symposium on Security and Privacy (SP)*, pp. 39–57. IEEE, 2017.

Pin-Yu Chen, Huan Zhang, Yash Sharma, Jinfeng Yi, and Cho-Jui Hsieh. Zoo: Zeroth order optimization based black-box attacks to deep neural networks without training substitute models. In *Proceedings of the 10th ACM Workshop on Artificial Intelligence and Security*, pp. 15–26. ACM, 2017.

Shuyu Cheng, Yinpeng Dong, Tianyu Pang, Hang Su, and Jun Zhu. Improving black-box adversarial attacks with a transfer-based prior. *arXiv preprint arXiv:1906.06919*, 2019.

Yinpeng Dong, Hang Su, Baoyuan Wu, Zhifeng Li, Wei Liu, Tong Zhang, and Jun Zhu. Efficient decision-based black-box adversarial attacks on face recognition. *arXiv preprint arXiv:1904.04433*, 2019.

Ian Goodfellow, Jonathon Shlens, and Christian Szegedy. Explaining and harnessing adversarial examples. In *International Conference on Learning Representations*, 2015. URL `http://arxiv.org/abs/1412.6572`.

Chuan Guo, Jacob R Gardner, Yurong You, Andrew Gordon Wilson, and Kilian Q Weinberger. Simple black-box adversarial attacks. *arXiv preprint arXiv:1905.07121*, 2019.

Kaiming He, Xiangyu Zhang, Shaoqing Ren, and Jian Sun. Deep residual learning for image recognition. In *Proceedings of the IEEE conference on computer vision and pattern recognition*, pp. 770–778, 2016.

Gao Huang, Zhuang Liu, Laurens Van Der Maaten, and Kilian Q Weinberger. Densely connected convolutional networks. In *Proceedings of the IEEE conference on computer vision and pattern recognition*, pp. 4700–4708, 2017.

Forrest N Iandola, Song Han, Matthew W Moskewicz, Khalid Ashraf, William J Dally, and Kurt Keutzer. Squeezenet: Alexnet-level accuracy with 50x fewer parameters and< 0.5 mb model size. *arXiv preprint arXiv:1602.07360*, 2016.

Andrew Ilyas, Logan Engstrom, Anish Athalye, and Jessy Lin. Black-box adversarial attacks with limited queries and information. In Jennifer Dy and Andreas Krause (eds.), *Proceedings of the 35th International Conference on Machine Learning*, volume 80 of *Proceedings of Machine Learning Research*, pp. 2137–2146, Stockholmsmässan, Stockholm Sweden, 10–15 Jul 2018. PMLR.

Alex Krizhevsky and Geoffrey Hinton. Learning multiple layers of features from tiny images. Technical report, Citeseer, 2009.

Alexey Kurakin, Ian Goodfellow, and Samy Bengio. Adversarial machine learning at scale. *arXiv preprint arXiv:1611.01236*, 2016.

Yann LeCun, Léon Bottou, Yoshua Bengio, Patrick Haffner, et al. Gradient-based learning applied to document recognition. *Proceedings of the IEEE*, 86(11):2278–2324, 1998.

Yandong Li, Lijun Li, Liqiang Wang, Tong Zhang, and Boqing Gong. Nattack: Learning the distributions of adversarial examples for an improved black-box attack on deep neural networks. *arXiv preprint arXiv:1905.00441*, 2019.

Yanpei Liu, Xinyun Chen, Chang Liu, and Dawn Song. Delving into transferable adversarial examples and black-box attacks. *arXiv preprint arXiv:1611.02770*, 2016.

Aleksander Madry, Aleksandar Makelov, Ludwig Schmidt, Dimitris Tsipras, and Adrian Vladu. Towards deep learning models resistant to adversarial attacks. In *International Conference on Learning Representations*, 2018. URL `https://openreview.net/forum?id=rJzIBfZAb`.

Seyed-Mohsen Moosavi-Dezfooli, Alhussein Fawzi, and Pascal Frossard. Deepfool: a simple and accurate method to fool deep neural networks. In *Proceedings of the IEEE conference on computer vision and pattern recognition*, pp. 2574–2582, 2016.

Jorge Nocedal. Updating quasi-newton matrices with limited storage. *Mathematics of computation*, 35(151):773–782, 1980.

Nicolas Papernot, Patrick McDaniel, and Ian Goodfellow. Transferability in machine learning: from phenomena to black-box attacks using adversarial samples. *arXiv preprint arXiv:1605.07277*, 2016a.

Nicolas Papernot, Patrick McDaniel, Somesh Jha, Matt Fredrikson, Z Berkay Celik, and Ananthram Swami. The limitations of deep learning in adversarial settings. In *2016 IEEE European Symposium on Security and Privacy (EuroS&P)*, pp. 372–387. IEEE, 2016b.

Olga Russakovsky, Jia Deng, Hao Su, Jonathan Krause, Sanjeev Satheesh, Sean Ma, Zhiheng Huang, Andrej Karpathy, Aditya Khosla, Michael Bernstein, et al. Imagenet large scale visual recognition challenge. *International journal of computer vision*, 115(3):211–252, 2015.

Mark Sandler, Andrew Howard, Menglong Zhu, Andrey Zhmoginov, and Liang-Chieh Chen. Mobilenetv2: Inverted residuals and linear bottlenecks. In *Proceedings of the IEEE Conference on Computer Vision and Pattern Recognition*, pp. 4510–4520, 2018.

Karen Simonyan and Andrew Zisserman. Very deep convolutional networks for large-scale image recognition. *arXiv preprint arXiv:1409.1556*, 2014.

Christian Szegedy, Wojciech Zaremba, Ilya Sutskever, Joan Bruna, Dumitru Erhan, Ian Goodfellow, and Rob Fergus. Intriguing properties of neural networks. In *International Conference on Learning Representations*, 2014. URL `http://arxiv.org/abs/1312.6199`.

Christian Szegedy, Wei Liu, Yangqing Jia, Pierre Sermanet, Scott Reed, Dragomir Anguelov, Dumitru Erhan, Vincent Vanhoucke, and Andrew Rabinovich. Going deeper with convolutions. In *Proceedings of the IEEE conference on computer vision and pattern recognition*, pp. 1–9, 2015.

Chun-Chen Tu, Paishun Ting, Pin-Yu Chen, Sijia Liu, Huan Zhang, Jinfeng Yi, Cho-Jui Hsieh, and Shin-Ming Cheng. Autozoom: Autoencoder-based zeroth order optimization method for attacking black-box neural networks. *arXiv preprint arXiv:1805.11770*, 2018.

Huaxia Wang and Chun-Nam Yu. A direct approach to robust deep learning using adversarial networks. In *International Conference on Learning Representations*, 2019. URL `https://openreview.net/forum?id=S1lIMn05F7`.

Chaowei Xiao, Bo Li, Jun-Yan Zhu, Warren He, Mingyan Liu, and Dawn Song. Generating adversarial examples with adversarial networks, 2018. URL `https://openreview.net/forum?id=HknbyQbC-`.

Cihang Xie, Yuxin Wu, Laurens van der Maaten, Alan Yuille, and Kaiming He. Feature denoising for improving adversarial robustness. *arXiv preprint arXiv:1812.03411*, 2018.

Saining Xie, Ross Girshick, Piotr Dollár, Zhuowen Tu, and Kaiming He. Aggregated residual transformations for deep neural networks. In *Proceedings of the IEEE conference on computer vision and pattern recognition*, pp. 1492–1500, 2017.

A Experiment Result

A.1 Targeted Attack On ImageNet

Figure 8 shows result of the targeted attack on dipper, American chameleon, night snake, ruffed grouse and black swan. TREMBA achieves much higher success rate than other methods at almost all queries level.

A.2 Un-targeted Attack on ImageNet

We used the same source model from targeted attack as the source model for un-targeted attack. We report our evaluation results in Table 5 and Figure 5. Compared with Trans-P-RGF, TREMBA reduces the number of queries by more than a half in ResNet34, DenseNet121 and MobilenetV2. Searching in the embedding space of generator remains very effective even when the target network architecture differs significantly from the networks in the source model.

Table 5: Success rate and average queries of un-targeted attack on ImageNet. $\varepsilon = 0.03125$

Attack	VGG19		Resnet34		DenseNet121		MobilenetV2	
	Success	Queries	Success	Queries	Success	Queries	Success	Queries
NES	**100%**	924	**100%**	1255	**100%**	1235	99.86%	872
Trans-NES$_{\text{PGD}}$	**100%**	441	**100%**	827	**100%**	838	**100%**	733
Trans-NES$_{\text{FGSM}}$	**100%**	586	**100%**	982	**100%**	961	**100%**	648
AutoZOOM	94.18%	5184	96.25%	3754	94.56%	4567	95.38%	4213
P-RGF	**100%**	277	99.72%	635	**100%**	709	99.72%	730
Trans-P-RGF	**100%**	130	99.86%	371	99.18%	806	99.86%	522
TREMBA	**100%**	**88**	**100%**	**183**	**100%**	**172**	**100%**	**61**

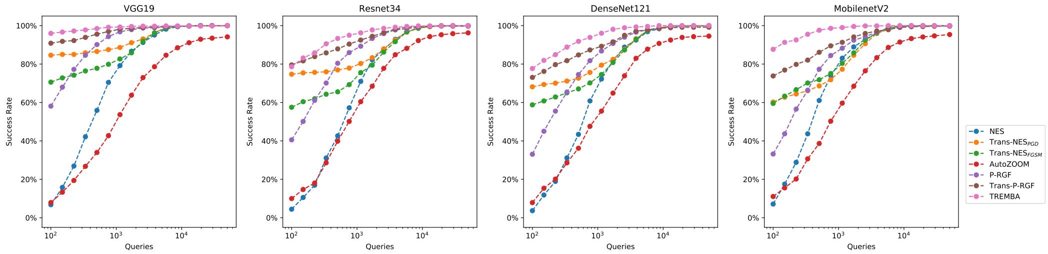

Figure 5: The success rate of un-targeted black-box adversarial attack at different query levels for undefended ImageNet models.

A.3 Visualization of targeted perturbation

Figure 9 shows some examples of adversarial perturbations produced by TREMBA. The first column is one image of the target class and other columns are examples of perturbations (amplified by 10 times). It is easy to discover some features of the target class in the adversarial perturbation such as the feather for birds and the body for snakes.

A.4 Experiments on Different Ensembles

We chose two more source ensemble models for evaluation. The first ensemble contains VGG16 and Squeezenet. And the second ensemble is consist of VGG16, Squeezenet and Googlenet. Figure 6 shows our result for targeted attack for ImageNet. We only compared Trans-NES$_{\text{PGD}}$ and Trans-P-RGF since they are the best variants from Trans-NES and P-RGF.

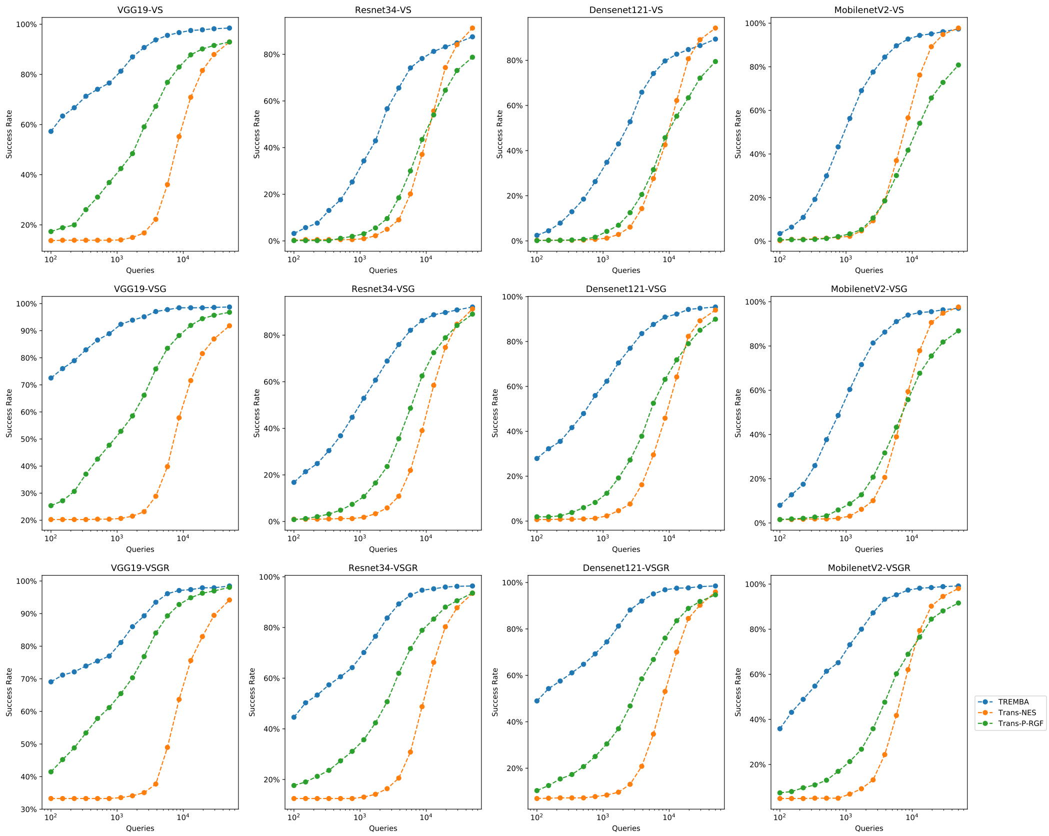

Figure 6: We show the success rate at different query levels for targeted attack for different ensemble source networks. V represents VGG16; S represents Squeezenet; G represents Googlenet; R represents Resnet18

A.5 Varying ε

We chose $\varepsilon = 0.02$ and $\varepsilon = 0.04$ and performed targeted attack on ImageNet. Although TREMBA used the same model that is trained on $\varepsilon = 0.03125$, it still outperformed other methods, which shows that TREMBA can also generalize to different strength of adversarial attack with different ε.

A.6 Varying sample size

We performed a hyperparameter sweep over b on Densenet121 on un-targeted attack on ImageNet. $b = 20$ may not be the best choice Trans-NES, but it is not the best for TREMBA, either. Generally, the performance is not very sensitive to b, and TREMBA will also outperform other methods even if we fine-tune the sample size for all the methods.

A.7 dimension of the embedding space

We slightly changed the architecture of the autoencoder by adding max pooling layers and changing the number of filters and perform un-targeted attack on ImageNet. More specifically, we added additional max pooling layers after the first and the fourth convolution layers and changed the number of filters of the last layer in the encoder to be 8. Thus, the dimension of the embedding space would be $8 \times 8 \times 8$. And we also changed the factor of bilinear sampling in the decoder. The remaining settings are the same in Appendix A.2. As shown in Table 7, this autoencoder is even worse than the original autoencoder despite small dimension of the embedding space. In addition, we also changed to dimension of the data-dependent prior of Trans-P-RGF to match the dimension of TREMBA,

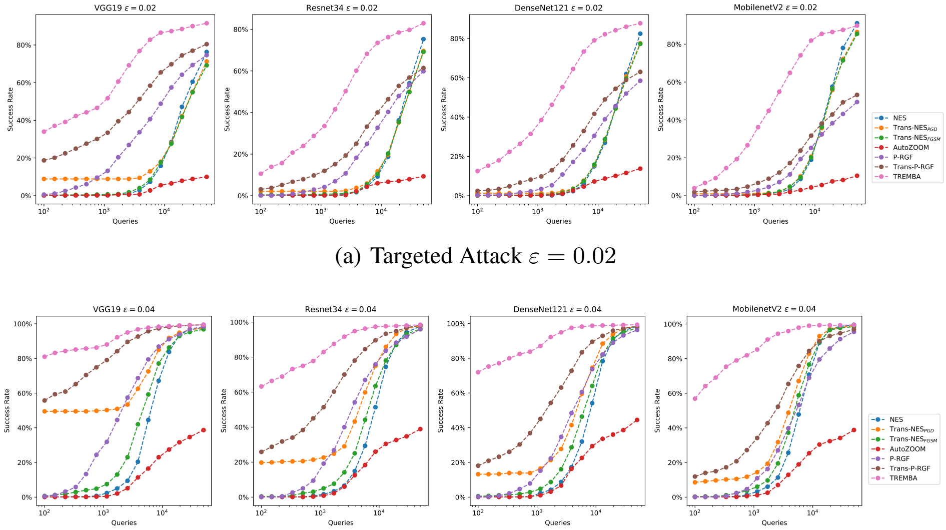

(a) Targeted Attack $\varepsilon = 0.02$

(b) Targeted Attack $\varepsilon = 0.04$

Figure 7: We show the success rate at different query levels for attack at different ε for ImageNet.

Table 6: Hyperparameter sweep over b on Densenet121 for un-targeted attack on ImageNet

Sweep over b	$b = 10$		$b = 30$		$b = 40$		$b = 50$	
	Success	Queries	Success	Queries	Success	Queries	Success	Queries
NES	100%	1323	100%	1284	100%	1433	100%	1639
Trans-NES$_{PGD}$	100%	915	100%	791	100%	707	100%	639
Trans-NES$_{FGSM}$	100%	1037	100%	916	100%	879	100%	886
AutoZOOM	90.9%	6052	96.2%	4148	97.1%	4066	97.3%	4366
P-RGF	99.73%	717	99.86%	860	99.86%	949	99.86%	1095
Trans-P-RGF	98.50%	1139	99.86%	479	99.86%	487	100%	427
TREMBA	100%	150	100%	205	100%	274	100%	299

Table 7: Change of dimension of the embedding space of AutoZOOM. The task is un-targeted attack on ImageNet.

Attack	VGG19		Resnet34		DenseNet121		MobilenetV2	
	Success	Queries	Success	Queries	Success	Queries	Success	Queries
AutoZOOM	64.35%	19684	71.94%	16931	68.44%	17871	71.15%	16134
Trans-P-RGF	99.86%	194	99.58%	508	99.59%	610	99.58%	705

whose performance is also not better than before. They show that simply diminishing the size of the embedding space may not lead to better performance. The performance gain of TREMBA comes beyond the effect of diminishing the dimension of the embedding space.

A.8 Examples of Attacking Google Cloud Vision API

Figure 10 shows one example of attacking Google Cloud Vision API. TREMBA successfully make the shark to be classified as green. Compared with Trans-NES$_{PGD}$, TREMBA hugely changes the labels of the image. It is hard to say the overall classification of Trans-NES$_{PGD}$ is wrong. However, the labels of TREMBA are definitely not correct.

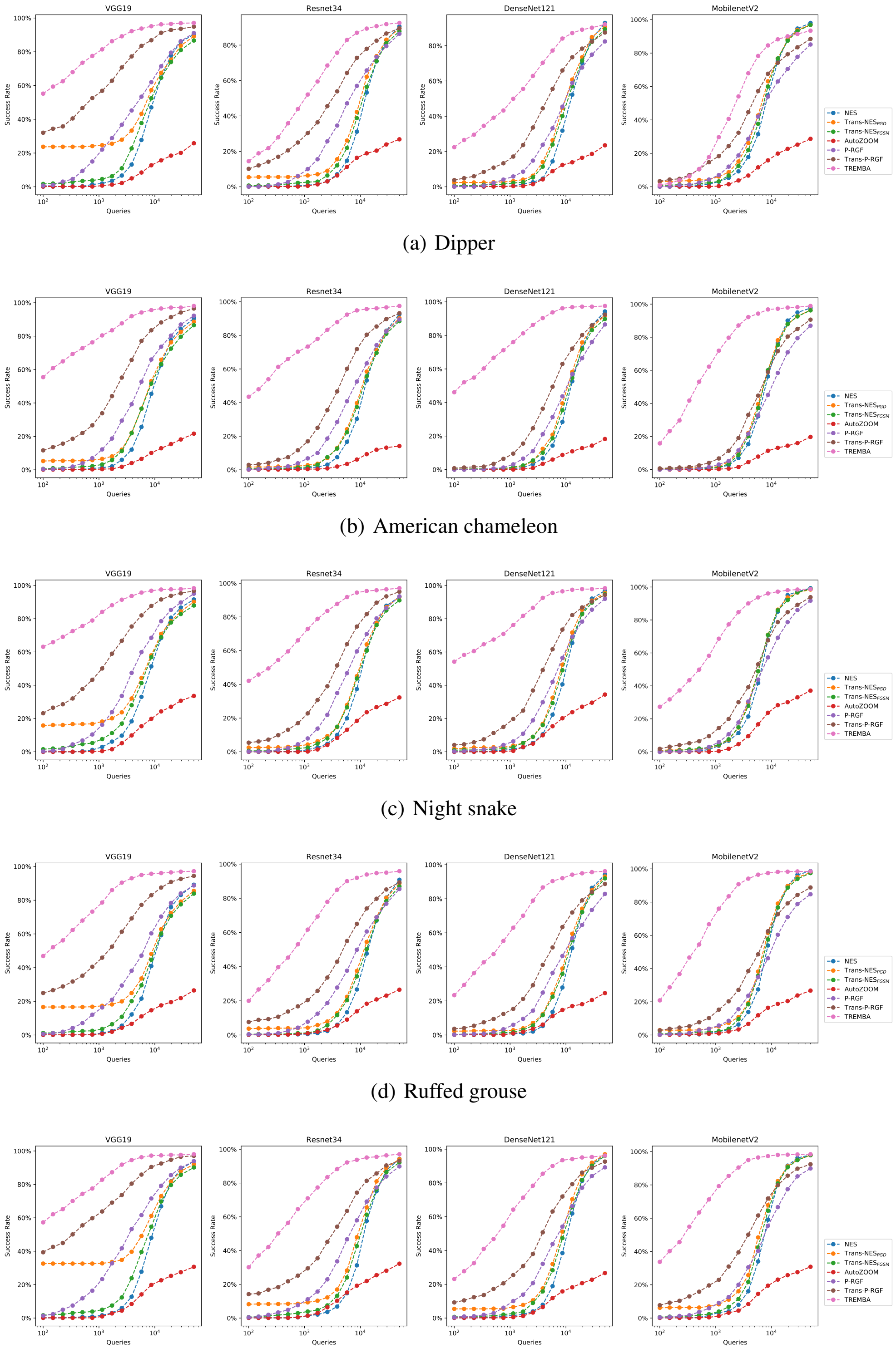

(a) Dipper

(b) American chameleon

(c) Night snake

(d) Ruffed grouse

(e) Black swan

Figure 8: The success rate at different query levels for attack targeted at different class. Targeted classes are: (a)Dipper; (b)American chameleon; (c)Night snake; (d)Ruffed grouse; (e)Black swan

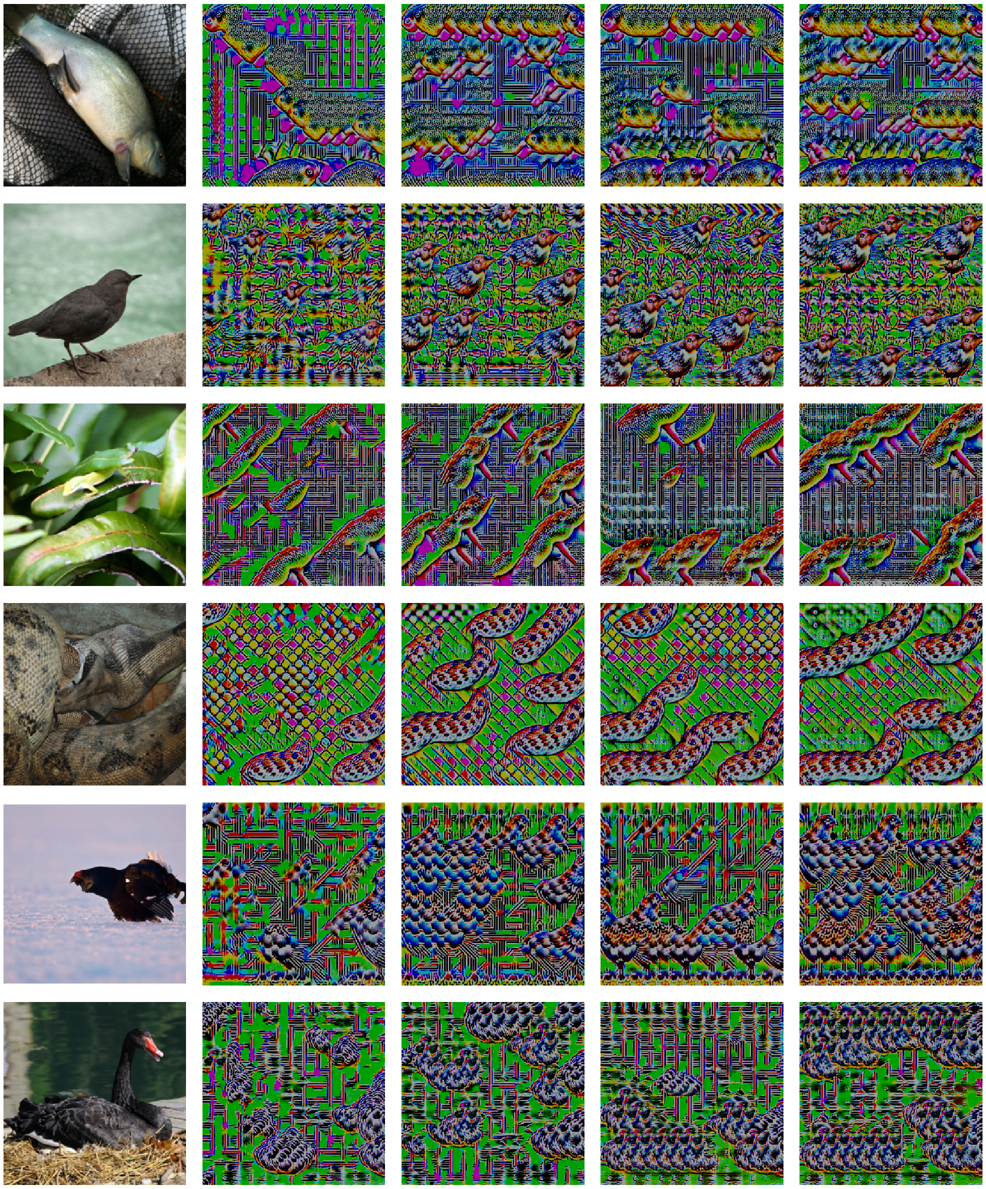

Figure 9: Visualization of adversarial perturbations for targeted attack on ImageNet. The first column shows one example of the target class. Other columns show the adversarial perturbations.

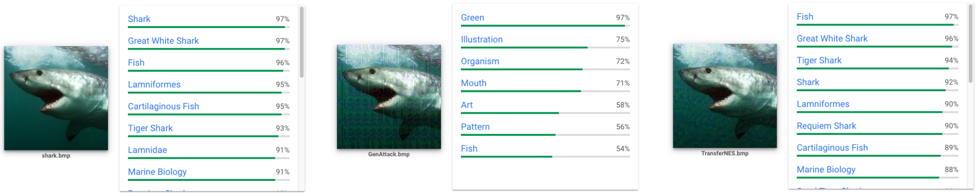

Shark	97%
Great White Shark	97%
Fish	96%
Lamniformes	95%
Cartilaginous Fish	95%
Tiger Shark	93%
Lamnidae	91%
Marine Biology	91%

Green	97%
Illustration	75%
Organism	72%
Mouth	71%
Art	58%
Pattern	56%
Fish	54%

Fish	97%
Great White Shark	96%
Tiger Shark	94%
Shark	92%
Lamniformes	90%
Requiem Shark	90%
Cartilaginous Fish	89%
Marine Biology	88%

(a) Origin Image (b) TREMBA (c) Trans-NES$_{\text{PGD}}$

Figure 10: One example of adversarial image for attacking Google Cloud Vision API

B Architecture of Classifiers and Generators

B.1 Classifier

Table 8: Model architectures for the MNIST

ConvNet1	ConvNet2	FCNet
Conv(64, 5, 5)+ReLU	Conv(16, 3, 3)+ReLU	FC(512)+ReLU
MaxPool(2,2)	Conv(16, 3, 3)+ReLU	FC(10)+Softmax
Conv(64, 5, 5)+ReLU	MaxPool(2,2)	
MaxPool(2,2)	Conv(32, 3, 3)+ReLU	
Dropout(0.25)	Conv(32, 3, 3)+ReLU	
FC(128)+ReLU	Conv(32, 3, 3)+ReLU	
Dropout(0.5)	MaxPool(2,2)	
FC(10)+Softmax	FC(512)+ReLU	
	FC(10)+Softmax	

Table 8 lists the architectures of ConvNet1, ConvNet2 and FCNet. The architecture of ResNeXt used in CIFAR10 is from `https://github.com/prlz77/ResNeXt.pytorch`. We set the depth to be 20, the cardinality to be 8 and the widen factor to be 4. Other architectures of classifiers are specified in the corresponding paper.

B.2 Generator

Table 9: Architectures of encoder and decoder. ConvReLUBN and DeconvReLUBN represent convolution or deconvolution followed by ReLU and batch normalization. The parameters (c, m, n) used in ConvReLUBN or DeconvReLUBN mean c channels with $m \times n$ kernel size. MaxPool(m, n) represents max pooling with (m, n) kernel size and (m, n) stride.

	MNIST	CIFAR10	ImageNet
Encoder	ConvReLUBN(16,3,3)	ConvReLUBN(16,3,3)	ConvReLUBN(16,3,3)
	ConvReLUBN(32,3,3)	ConvReLUBN(32,3,3)	ConvReLUBN(32,3,3)
	ConvReLUBN(32,3,3)	ConvReLUBN(32,3,3)	MaxPool(2,2)
	MaxPool(2,2)	MaxPool(2,2)	ConvReLUBN(64,3,3)
	ConvReLUBN(32,3,3)	ConvReLUBN(32,3,3)	ConvReLUBN(64,3,3)
	ConvReLUBN(16,3,3)	ConvReLUBN(32,3,3)	MaxPool(2,2)
	ConvReLUBN(2,3,3)	ConvReLUBN(8,3,3)	ConvReLUBN(128,3,3)
	MaxPool(2,2)	MaxPool(2,2)	ConvReLUBN(128,3,3)
			MaxPool(2,2)
			ConvReLUBN(32,3,3)
			ConvReLUBN(8,3,3)
			MaxPool(2,2)
Decoder	ConvReLUBN(32,3,3)	ConvReLUBN(32,3,3)	ConvReLUBN(32,3,3)
	ConvReLUBN(32,3,3)	ConvReLUBN(32,3,3)	DeconvReLUBN(64,3,3)
	DeconvReLUBN(64,3,3)	DeconvReLUBN(64,3,3)	ConvReLUBN(128,3,3)
	ConvReLUBN(64,3,3)	ConvReLUBN(64,3,3)	DeconvReLUBN(128,3,3)
	ConvReLUBN(64,3,3)	ConvReLUBN(64,3,3)	ConvReLUBN(128,3,3)
	DeconvReLUBN(16,3,3)	DeconvReLUBN(16,3,3)	DeconvReLUBN(64,3,3)
	Conv(1,1,1)	Conv(3,1,1)	ConvReLUBN(32,3,3)
			DeconvReLUBN(16,3,3)
			ConvReLUBN(3,1,1)

Table 9 lists the architectures of generator for three datasets. For AutoZOOM, we find our architectures are not suitable and use the same generators in the corresponding paper.

C Hyperparameters

C.1 Training Generator

We trained the generators with learning rate starting at 0.01 and decaying half every 50 epochs. The whole training process was 500 epochs. The batch size was determined by the memory of GPU. Specifically, we set batch size to be 256 for MNIST and CIFAR10 defense model, 64 for ImageNet model. All large κ will work well for our method and we chose $\kappa = 200.0$. All the experiments were performed using *pytorch* on NVIDIA RTX 2080Ti.

C.2 Evaluation

Table 10 to 15 list the hyperparameters for all the algorithms. The learning rate was fine-tuned for all the algorithms. We set sample size $b = 20$ for all the algorithms for fair comparisons.

Table 10: Hyperparameters for NES

	MNIST	CIFAR10	ImageNet		
			Un-targeted	Targeted	Un-targeted Defense
Sample size (b)	20	20	20	20	20
Learning rate (η)	0.2	0.05	0.1	0.05	0.1

Table 11: Hyperparameters for Trans-NES$_{\text{PGD}}$ and Trans-NES$_{\text{FGSM}}$. White-box iteration, white-box margin and white-box learning rate mean the hyperparameters for generating the starting point on the source network for Trans-NES$_{\text{PGD}}$.

	MNIST	CIFAR10	ImageNet		
			Un-targeted	Targeted	Un-targeted Defense
Sample size (b)	20	20	20	20	20
Learning rate (η)	0.2	0.05	0.1	0.05	0.1
White-box iteration	50	100	50	50	100
White-box margin(κ)	100	100	100	100	100
White-box learning rate	0.05	0.1	0.01	0.005	0.1

Table 12: Hyperparameters for AutoZOOM.

	MNIST	CIFAR10	ImageNet		
			Un-targeted	Targeted	Un-targeted Defense
Sample size (b)	20	20	20	20	20
Learning rate (η)	5.0	20.0	5.0	3.0	5.0

Table 13: Hyperparameters for P-RGF and Trans-P-RGF.

	MNIST	CIFAR10	ImageNet		
			Un-targeted	Targeted	Un-targeted Defense
Sample size (b)	20	20	20	20	20
Learning rate (η)	0.1	0.05	0.005	0.003	0.005
White-box iteration	50	100	50	50	100
White-box margin(κ)	100	100	100	100	100
White-box learning rate	0.05	0.1	0.01	0.01	0.1

Table 14: Hyperparameters for TREMBA.

	MNIST	CIFAR10	ImageNet		
			Un-targeted	Targeted	Un-targeted Defense
Sample size (b)	20	20	20	20	20
Learning rate (η)	0.3	2.0	5.0	3.0	5.0

Table 15: Hyperparameters for TREMBA$_{\text{OSP}}$.

	CIFAR10 Defense	ImageNet Defense
Sample size (b)	20	20
Learning rate (η)	2.0	5.0
White-box iteration	100	100
White-box margin(κ)	100	100
White-box learning rate	1.0	2.0